
Article:
Yeardley, A.J., Bugryniec, P.J., Milton, R.A. et al. (1 more author) (2020) A study of the thermal runaway of lithium-ion batteries : a Gaussian process based global sensitivity analysis. Journal of Power Sources, 456. 228001. ISSN 0378-7753

https://doi.org/10.1016/j.jpowsour.2020.228001

A Study of the Thermal Runaway of Lithium-ion Batteries: A Gaussian Process based Global Sensitivity Analysis

Aaron S. Yeardley, Peter J. Bugryniec, Robert A. Milton, Solomon F. Brown*

Department of Chemical and Biological Engineering, The University of Sheffield, Sheffield S10 2TN

Abstract

A particular safety issue with Lithium-ion (Li-ion) cells is thermal runaway (TR), which is the exothermic decomposition of cell components creating an uncontrollable temperature rise leading to fires and explosions. The modelling of TR is difficult due to the broad range of cell properties and potential conditions. Understanding the effect that thermo-physical and heat transfer characteristics have on the TR abuse model output is essential to develop more accurate and robust TR models. This study uses global sensitivity analysis (GSA) to investigate the effect of the cell parameters on the outcome of TR events. Using a Gaussian Process (GP) surrogate model to calculate the Sobol' indices, it is shown that the emissivity value is the dominant thermo-characteristic throughout the overall abuse scenario. Further analysis, investigating three key TR features shows the conductivity coefficient to be the most important with respect to the maximum temperature reached during TR. Results demonstrate that researchers can confidently estimate some thermo-characteristics but require accurate characterisation of the emissivity and conductivity coefficient to ensure robust predictions. Given the importance of battery technology to aid in global de-carbonisation, these findings are key to increasing their safe design and operation.

Keywords: Gaussian Process, Thermal Runaway, Sobol' Indices, Global Sensitivity Analysis, Li-ion Cells

1. Introduction

Lithium-ion (Li-ion) cells are an increasingly popular electrochemical storage device (Steen et al., 2017; Kim et al., 2012; International Energy Agency, 2016) which play a pivotal role in applications such as electric vehicles and grid energy storage. Li-ion cells have been extensively studied in order to increase cell performance (Nitta et al., 2015; Ghadbeigi et al., 2015), reduce cell cost (Nitta et al., 2015), reduce environmental impact (Peters et al., 2017) and improve safety (Abada et al., 2016). However, a particular issue with Li-ion cells is thermal runaway (TR) which is the exothermic decomposition of cell components creating an uncontrollable rise in temperature leading to fires

*Corresponding author.
E-mail address: s.f.brown@sheffield.ac.uk

and explosions (Wang et al., 2012; Larsson et al., 2018; Feng et al., 2018). Hence, understanding the TR process, to prevent it occurring or reducing its severity, is essential for the development of safer batteries.

Current literature focuses on the development of models designed for carrying out studies to determine the effects of cell design (Kim et al., 2007; Lopez et al., 2015; Hu et al., 2017), environmental and abuse conditions (Chiu et al., 2014; Lopez et al., 2015) and pack design (Coleman et al., 2016; Xu et al., 2017; Duan et al., 2018) on TR behaviour or prevention. Recent studies have explored the implications of using Li-ion batteries in extreme environments, investigating how severe irradiation can cause TR (Shack et al., 2014; Ma et al., 2017; Wu et al., 2019). Yet little work has been carried out to understand the uncertainties within TR modelling and/or how variance in the physical parameters can affect the temperature during a TR event.

The need to understand TR events in Li-ion cells has motivated the development of physics-based models to provide assistance in the analysis of the mechanics allowing a more cost-effective and safer method rather than iterating cell abuse experimentally. As a result, research has been undertaken with various approaches based on the Arrhenius formulation of cell decomposition reactions and heat generation (Hatchard et al., 2001; Kim et al., 2007; Lopez et al., 2015) to develop computational models of TR in cells with studies. For example, comparing cell chemistry (Peng and Jiang, 2016), utilising efficiency factors for the conversion of electrochemical energy to thermal energy (Coman et al., 2017), and the effect of nail penetration (Chiu et al., 2014). Previous work utilises an accelerated rate calorimeter (ARC) to determine the initial reaction kinetics of the solid electrolyte interface (SEI) and cathode reactions of cells (Richard and Dahn, 1999a; MacNeil et al., 2000). Mao et al. (2020) also used an ARC to investigate the self-heating reaction and TR criticality of Li-ion cells resulting in kinetic data that will aid in future modelling of Li-ion battery safety. Additionally, inverse modelling techniques have been used to estimate the parameters involved in the reaction kinetics for both cell components (Richard and Dahn, 1999b; MacNeil et al., 2000) and full cells (Ren et al., 2018; Liu et al., 2018). Liu et al. (2018) developed a one reaction model for an entire cell which takes into account the state of charge (SOC) by fitting experimental ARC data at different SOC's to determine the parameters of the Arrhenius equation and the heat of reaction as a third-order polynomial which is a function of SOC. Ren et al. (2018) determined parameter values through Kissinger and nonlinear fitting methods of direct scanning calorimetry (DSC) data. Fundamental thermal abuse experiments of ARC, DSC and oven exposure are used to validate such computational models. However, the TR models developed for Lithium iron phosphate (LFP) cells (Peng and Jiang, 2016) have not been validated well as inaccuracies are found when compared to new experimental work (Bugryniec et al., 2019). Therefore, the need to develop computational models of TR events are strained by the lack of understanding in the model parameters meaning an intensive study of the parameter sensitivities is essential for a thorough understanding of the TR of Li-ion cells.

A sensitivity analysis (SA) characterises the relationship between a system's inputs and outputs thus showing how the uncertainty of the outcome can be apportioned to the different sources of uncertainty in the input. This will provide important knowledge in relation to the safety and development of Li-ion cells given that:

1. Parameters are commonly estimated within TR models if they cannot be measured or have no measured values available in the literature,

2. There is an unknown certainty of the appropriateness of values in the literature for parameters such as composite materials i.e. electrodes, or for the overall cell properties. Especially when considering that exact cell compositions for literature sources or cells under study may be unknown. For example, Liu et al. (2018) and Drake et al. (2014) have both calculated the specific heat capacity of an 18650 LFP cell but resulted in different values. Various other literature have recorded a specific heat capacity ranging from $1100\,\mathrm{J\,kg^{-1}\,K^{-1}}$ to $1720\,\mathrm{J\,kg^{-1}\,K^{-1}}$ (Spinner et al., 2015; Wang et al., 2013; Chen et al., 2005a). Highlighting the significant variation, in just one parameter, of which the authors here have found that a 10% change can lead to significant variations in the TR simulation results.

3. Carrying out SA studies can help future developments, as the uncertainty in the model can be related to a real change in a physical cell.

This work will analyse the thermo-physical and heat transfer characteristics of a TR model to determine their influence on cell temperature under external heating of an LFP cell leading to a TR event. The focus is on an LFP cell as a case study due to it being considered the safest Li-ion chemistry (Jiang and Dahn, 2004; Bugryniec et al., 2018, 2019). SA has been implemented in many different research fields (for example Saltelli et al., 2005; Rohmer and Foerster, 2011; Al et al., 2019) as it is widely acknowledged as a good practice to better understand model behaviour. Specifically for battery research, sensitivity studies have been employed to advance the development and design of battery performance (Drews et al., 2003; Schmidt et al., 2010; Vazquez-Arenas et al., 2014; Zhang et al., 2014) without considering TR event occurring. Additionally, these sensitivity studies focused on minor parameter changes and how it affects the variation in the model output using a local SA study. In general, the most common class of SA method is the global sensitivity analysis (GSA) because it looks at the model behaviour over the whole range of inputs and outputs. Unlike other methods, such as local SA, GSA quantifies the variation of the model response in the entire parameter domain fully exploring the input space. The first example, to the authors knowledge, to practise a GSA for battery development was Trembacki et al. (2016), where polynomial chaos expansion was used to calculate sensitivity index values for a thermal simulation of molten salt batteries. Recent literature by Lin et al. (2018) has applied a GSA to a large scale multiphysics Li-ion battery model. The SA was achieved by calculating the Sobol' indices using a

polynomial chaos expansion approach to surrogate the 3D multiphysics model. Specifically, the safety of an LFP cell has been explored using GSA by Rajan et al. (2018) who considered the displacement, temperature and strain rate of a battery with respect to it's mechanical strength when subjected to external impacts that lead to TR. The research conducted a SA using an artificial neural network to emulate a finite element model and showed the temperature of a cell to have the most influence on the mechanical strength leading to catastrophic TR explosions. Whereas, the TR process of a Li-ion cell has only been analysed once with respect to sensitivity studies, when GPs were used as a surrogate model to optimise the reaction parameters in a TR abuse simulation (Milton et al., 2019). The work used the error of a heuristic fit (RMSE) between simulated and experimental results as an output to a GP, which was further reduced by an optimal rotation of the input basis. The input variables being optimised, were the parameters that control the reactions which govern the heat generation in the TR model.

The methodology presented in this work will use the Sobol' sensitivity indices, which are a variance-based decomposition method that is considered the benchmark for GSA methods (Rohmer and Foerster, 2011; Al et al., 2019). However, the calculation of Sobol' indices require a significant number of model evaluations to ensure convergence to a satisfactory precision level. Hence, the computational burden can be reduced by using meta-modelling techniques such as the polynomial chaos expansion (Brown et al., 2013; Sudret, 2008), artificial neural networks (Li et al., 2016), and Gaussian Processes (GPs) (Marrel et al., 2009). Here, based on our previous work, the surrogate model will be developed using GPs as they are a widely used tool for Bayesian nonlinear regression and provide an approach that predicts a distribution allowing uncertainties for each prediction. This novel approach will allow us to determine:

- which of the thermo-physical and heat transfer characteristics contribute most to the temperature output variability with respect to the time during a TR simulation,
- the number of interactions between the thermo-characteristics and with which inputs,
- which properties are insignificant and so do not need to be well characterised, helping to simplify TR models.

These goals are achieved by developing a TR model of an LFP cell which is emulated by a GP surrogate model enabling the calculation of Sobol' indices.

This work is organised as follows. Section 2 describes the methodology and the mathematics behind the three techniques before the results sections consist of the analysis of the three tools. First, the TR model is compared to experimental data, ensuring it accurately represents a real cell under TR allowing GPs to be created for a time-dependent SA on the temperature of a cell. The role of the thermo-characteristics on TR behaviour is then further investigated with analysis of the time at which self-heating and TR begins, as well as the the maximum temperature reached by the TR event. Once the GP's were produced, each one had to be validated ensuring inaccuracies were

not carried over to the calculation of the Sobol' indices. The final results from the GSA presents the time-dependent Sobol' indices and the Sobol' indices from the three TR features. The report is then concluded in Section 4 detailing how the resulting sensitivity measures can guide the decision-making process when designing Li-ion cells and their models.

2. Methodology

This section presents the TR model, developed for an LFP cell, before it describes the formulation of the GP emulators and the calculation of the Sobol' indices.

2.1. TR Model

The TR abuse model for the LFP cell is constructed in the commercial finite element modelling software *COMSOL Muiltiphysics 5.2a* (COMSOL Multiphysics®V5.2a). The governing equations for heat transfer utilises one-dimensional forms of Fourier's law of heat conduction, Newton's law of cooling for convection and Stefan-Boltzmann equation for radiation (for example Kim et al., 2007). The model represents an 18650 LFP cell (1.5 Ah) under oven exposure with free convection. The model assumes a 1D axi-symmetric geometry, consisting of three geometric domains; the mandrel, the jelly roll (the coil of electrodes, separator and current collector layers) and the cell casing, see Figure 1. The multilayer jelly roll is assumed to be constituted of a single homogeneous material to reduce computational complexity. This is to allow the use of measured properties of an entire cell and also to reduce model input parameters. Further, the model assumes all geometric domains take the average material values of a whole cell, as these are more accurately available, and it also reduces model input parameters.

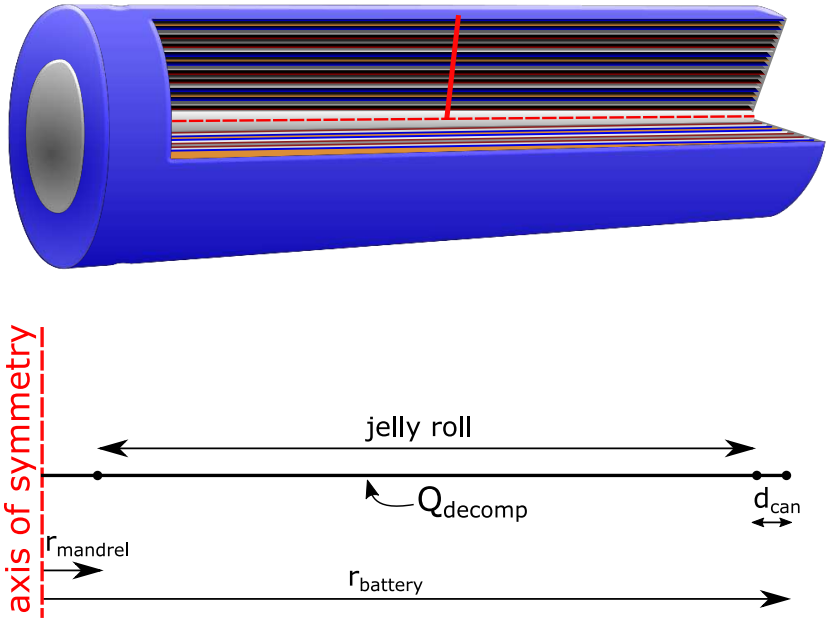

Figure 1: Top) Representation of a 18650 cell indicating (by the red line) the model simplification, bottom) schematic of model geometry.

Heat transfer in the model assumes a solid body throughout and considers conduction throughout the cell, while at the cells' surface free convection and radiation are considered. The exothermic decomposition reactions driving TR are described by individual Arrhenius equations. Here the four common reactions are considered, these are the SEI decomposition, the negative electrode reaction (NE), positive material decomposition (PE) and electrolyte decomposition (E) (Spotnitz and Franklin, 2003), while the total decomposition heat is the summation of these individual heat generation terms. This decomposition heat is assumed to be distributed over the entire jelly roll domain. The formulation of these governing reactions follows that outlined by Kim et al. (2007).

The rate of reaction, R_x (s^{-1}), for the SEI, positive and electrolyte reactions is given by:

$$R_x = A_x e^{\left(\frac{-E_{a,x}}{RT}\right)} C_x^{m_x} \left(1 - C_x\right)^{n_x} \tag{1}$$

where subscript x corresponds to one of the reactions sei, pe or e. A_x (s^{-1}) is the frequency factor, $E_{a,x}$ ($\mathrm{J\,mol}^{-1}$) is the activation energy, R and T the ideal gas constant ($8.3145\,\mathrm{J\,mol}^{-1}\,\mathrm{K}^{-1}$) and temperature (K) respectively, dimensionless quantities include: C_x the reaction species, while n_x and m_x are constants.

The negative electrode reaction is of a similar form:

$$R_{ne} = A_{ne} e^{\left(\frac{-E_{a,ne}}{RT}\right)} C_{ne}^{m_{ne}} \left(1 - C_{ne}\right)^{n_{ne}} e^{\left(\frac{-t_{sei}}{t_{sei,0}}\right)} \tag{2}$$

with the additional term, t_{sei}, a non-dimensional representation of the change in thickness of the SEI layer as it decomposes. $t_{sei,0}$ the initial thickness. The change in reaction species for each decomposition reaction and SEI layer thickness is given by:

$$\frac{\partial C_{sei}}{\partial t} = -R_{sei} \tag{3}$$

$$\frac{\partial C_{ne}}{\partial t} = -R_{ne} \tag{4}$$

$$\frac{\partial t_{sei}}{\partial t} = R_{ne} \tag{5}$$

$$\frac{\partial C_{pe}}{\partial t} = R_{pe} \tag{6}$$

$$\frac{\partial C_{e}}{\partial t} = -R_{e} \tag{7}$$

The volume-specific heat generation terms Q_z (W m^{-3}) from each decomposition reaction are given by:

$$Q_z = H_z W_y R_z \tag{8}$$

where H_z (J kg^{-1}) is the specific heat of reaction for reactions $z = sei, ne, pe, e$ and W_y (kg m^{-3}) is the volume-specific content of reactive material, i.e. $y = c, p, e$ corresponding to carbon active material, positive active material and electrolyte respectively. W_c is used in the SEI and NE heat generation equations, W_p in the PE heat generation equation and W_e in the electrolyte heat generation equation.

Hence, the total heat generation from the decomposition of the cell is:

$$Q_{decomp} = Q_{sei} + Q_{ne} + Q_{pe} + Q_e \tag{9}$$

The thermo-physical parameters and heat transfer parameters are initially taken from experimental findings in the literature and are presented in Table 1. The parameters for the decomposition equations are estimated through comparison with experimental data and are presented in Table 2. Parameters describing the cell geometry, initial temperature and oven temperature and simulation time are presented in Table 3.

Table 1: Thermo-physical and heat transfer characteristics.

Parameter	**Reference value**	**Range**	**STD**
$\rho(\mathrm{kg\,m^{-3}})$	2418 [a]	2413 - 2426[a]	4.260[a]
$C_p(\mathrm{kJ\,kg^{-1}\,K^{-1}})$	1105 [a]	1092 - 1115[a]	8.680[a]
$h_{conv}(\mathrm{W\,m^{-2}\,K^{-1}})$	12.5 [b]	7.00 - 12.5[c]	1.00[d]
$\kappa_r(\mathrm{W\,m^{-1}\,K^{-1}})$	0.5 [d]	0.2 - 3[c]	0.1[d]
ε	0.8 [b]	0 - 1	0.1[d]

[a] Measured and calculated experimentally (Bugryniec et al., 2019)

[b] Reference value from Hatchard et al. (2001)

[c] Literature ranges Refs. (Guo et al., 2010; Hatchard et al., 2001; Kim et al., 2007; Hatchard et al., 2000; Dong et al., 2018; Coman et al., 2017; Liu et al., 2018; Zhao et al., 2014; Tanaka and Bessler, 2014)

[d] Estimated

Table 2: Kinetic parameters used in the decomposition equations.

Kinetic Parameter	**Carbon**	**SEI**	**$LiFePO_4$**	**Electrolyte**
Frequency Factor, $A(\mathrm{s^{-1}})$	2.50×10^{13}	1.67×10^{15}	2.00×10^{8}	5.14×10^{25}
Activation Energy, $E_a(\mathrm{J\,mol^{-1}})$	1.42×10^{5}	1.50×10^{5}	9.60×10^{4}	2.82×10^{5}
Reaction order, m	1.00	1.00	1.00	1.00
Reaction order, n	0.00	0.00	1.00	0.00
Heat, $H(\mathrm{J\,g^{-1}})$	1714	578.0	194.7	645.0
Specific weight, $W(\mathrm{kg\,m^{-3}})$	560	560	977	151
Species initial values, C_x, t_{sei}	0.75 ($t = 0.33$)	0.15	0.040	0.99

Table 3: Additional simulation parameters.

Parameter	**Value**
$\mathrm{r_{bat}}$ (mm)	18
$\mathrm{r_{man}}$ (mm)	2
$\mathrm{d_{can}}$ (mm)	0.3
$\mathrm{T_{int}}$ $(°C)$	16.5
$\mathrm{T_{oven}}$ $(°C)$	218
$\mathrm{t_{length}}$ (min)	90

Due to the uncertainty in the experimental data, ranges for the thermo-physical and heat transfer characteristics (density, heat capacity, convection coefficient, radial thermal conductivity and emissivity value) were defined, while the abuse parameters were kept constant. The initial values (used in the parameter estimation of the model) of the varied parameters are taken to be the mean of the normal distribution. The standard deviation of the density and heat capacity is calculated from experimental findings, while the standard deviation of the convection coefficient, conductivity value and emissivity value are estimated arbitrarily by setting it to 1 relative to the order of magnitude. A random sampling of these five parameters is undertaken using Latin Hypercube Sampling (LHS) (Stein, 1987), normally distributed about the mean, and used to generate 753 sample points in the input space. Note that as emissivity has physical limits between 0 and 1, any parameter sets that have an emissivity value out of this range are removed, leading to a curtailment of the final distribution of emissivity values. Each of these 753 parameter sets is used (in conjunction with the original estimated abuse parameters) to carry out an oven simulation at $218°C$ exposure. The resulting temperature data and initial input parameters sets are used to train a GP as described in the previous section.

2.2. GP Surrogate Model

In this study, standard Bayesian conditioning is used to take Gaussian priors and derive a predictive process. This allows the creation of a GP which takes a $(1 \times d)$ row vector of inputs $\mathbf{x}$ and returns a Gaussian random variable through calculations using the predictive equations

$$y(\mathbf{x}) \sim \mathsf{N}\left[\bar{f}(\mathbf{x}), \Sigma_y + \sigma_e^2\right] \tag{10}$$

where

$$\bar{f}(\mathbf{x}) := k(\mathbf{x}, \mathbf{X})(k(\mathbf{X}, \mathbf{X}) + \sigma_e^2 \mathbf{I})^{-1}\mathbf{y} = k(\mathbf{x}, \mathbf{X})\mathbf{K}^{-1}y \tag{11}$$

$$\Sigma_y := k(\mathbf{x}, \mathbf{x}) - k(\mathbf{x}, \mathbf{X})(k(\mathbf{X}, \mathbf{X}) + \sigma_e^2 \mathbf{I})^{-1}k(\mathbf{X}, \mathbf{x}) = k(\mathbf{x}, \mathbf{x}) - k(\mathbf{x}, \mathbf{X})\mathbf{K}^{-1}k(\mathbf{X}, \mathbf{x}) \tag{12}$$

whose mean $\bar{f}(\mathbf{x})$ and variance Σ_y is learnt from training data $\mathbf{y} = f(\mathbf{X}) + \mathbf{e}$. Standard Bayesian inference has been used to express the mean prediction in terms of the $(n \times 1)$ observed responses $\mathbf{y}$ to $(n \times d)$ training inputs $\mathbf{X}$. At the heart of this lies the kernel function $k\colon \mathbb{R}^{i+d} \times \mathbb{R}^{j+d} \to \mathbb{R}^i \times \mathbb{R}^j$, expressing the correlation between responses to input samples of sizes $(i \times d)$ and $(j \times d)$; for the purposes of this work the number of input dimensions is $d = 5$. This work exclusively uses the automatic relevance determination (ARD) kernel (Wipf and Nagarajan, 2007):

$$k(\mathbf{x}', \mathbf{x}) := \sigma_f^2 \exp\left(-\frac{(\mathbf{x} - \mathbf{x}')\Lambda^{-2}(\mathbf{x} - \mathbf{x}')^\intercal}{2}\right) \tag{13}$$

where Λ is a $(d \times d)$ *diagonal* positive definite lengthscale matrix. The learning from training data requires the optimisation $d+2$ hyperparameters, constituting of Λ, σ_f, and σ_e, through the maximum marginal likelihood $p[\mathbf{y}|\mathbf{X}]$ using the ROMCOMMA software library (ROMCOMMA, 2019).

2.3. Sobol' Indices

In this work, the approach to the calculation of the Sobol' indices follows Jin et al. (2004) by substituting the true simulation model with the mean of the conditional GP resulting in semi-analytic Sobol' indices. This section will describe the calculation of Sobol' indices up to evaluating integrals, which will be evaluated using the GP surrogate model to allow more efficient computation.

Sobol' indices are calculated by considering a function $y = f(\mathbf{x})$, where $\mathbf{x} := [x_1, ..., x_d]$ is a d-dimensional row vector found in the input space, Ω, and y is the model output. Assuming that the inputs are mutually dependent and that $f(\mathbf{x}) \in L^2(\Omega)$ (Sobol, 1993, 2001). For a particular input x_i, it's first-order Sobol' index is defined by

$$S_{1,i} = \frac{Var\{E(y|x_i)\}}{Var\{y\}} = \frac{D_i}{D} \tag{14}$$

Then second-order Sobol' indices between input i and j shows the interactions between x_i and x_j:

$$S_{2,ij} = \frac{Var\{E(y|x_i x_j)\} - Var\{E(y|x_i)\} - Var\{E(y|x_j)\}}{Var\{y\}} = \frac{D_{ij}}{D} \tag{15}$$

To be able to express the whole effect of an input on the output, the total Sobol' index is (Saltelli and Homma, 1996)

$$S_{T,i} = S_{1,i} + \sum_{j \neq i}^{n} S_{2,ij} + \sum_{j \neq i, k \neq i, j<k}^{n} S_{3,ijk} + ... \tag{16}$$

Therefore, the first-order Sobol' indices measure the contribution to the variance solely attributable to x_i, in contrast, the total Sobol' index of i corresponds to its own contribution including interactions with the other inputs.

From here, the partial variances of y are determined through a decomposition method presented by Sobol (1993) which evaluates each term through multidimensional integrals. As previously mentioned in Section 1, here we use a GP surrogate model to calculate the Sobol' sensitivity indices by using Equation (11), the GP predictive mean, to analytically compute the integrals. Therefore, we have calculated the Sobol' indices of the predicted value so that $y = \bar{f}(\mathbf{x})$, in a similar way to that from Chen et al. (2005b).

3. Results

This section presents the results of the GSA of the LFP TR as described in the previous section. The case study considers a commercial $1500\ mAh$ 18650 $3.2V$ $LiFePO_4$ cell, and begins with an analysis of the full order model results providing further understanding of the distribution of the data. Following this, the analysis is split into two sections, first the time-dependent temperature analysis and then the TR features analysis. Both sections include cross-validation of a GP surrogate model to assess it's predictive accuracy and reliability. A full SA is presented including both the first order and the total Sobol' indices in an attempt to understand the thermo-physical and heat transfer characteristics that govern TR. Finally, the GSA is efficiently analysed by comparing the Sobol' sensitivity indices for the inputs to further understand which properties govern the TR process. In particular, the research is focused on understanding the temperature-time profile during TR and so the maximum temperature reached (the TR severity) is detailed as much as the time to TR.

3.1. Full Order Model

Figure 2 shows the predicted cell surface temperature when exposing an LFP cell to an oven temperature of $218°C$ when simulating using the estimated abuse parameters from Table 2 and the reference values for the thermo-physical and heat transfer characteristics shown in Table 1. The simulated fit is compared to an unpublished experimental dataset produced using an oven test that follows the methodology from Bugryniec et al. (2019). The simulation produces the general cell TR behaviour well, while specific details such as time to TR and TR severity are not accurately predicted. However, in the context of this work, utilising a TR model to produce a data set for SA and to produce more general comments for TR model development, the model is deemed appropriate for the remainder of this work.

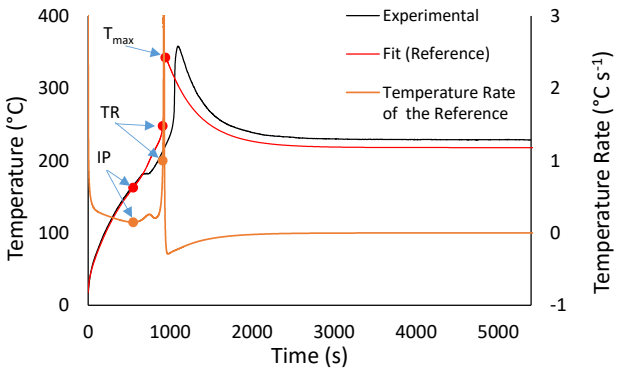

Figure 2: Full order model prediction of an LFP cell TR event due to oven exposure at $218°C$ and compared to experimental results.

Figure 3 shows the mean cell surface temperature of all 753 runs varying with time, alongside the original (refer-

ence) temperature profile for comparison. Also shown are the upper and lower bounds of the simulation results, i.e the mean plus and minus 2 standard deviations (STDs) respectively, while the value of the STD with time is also plotted. The difference between the mean and reference plots, as well as the magnitude and variation of the STD show how the predicted cell temperature is effected by simply changing the thermo-physical and heat transfer characteristics. Figure 3 highlights what is referred to as the "TR event", importantly both before and after the TR event the mean results of the temperature profile are close to the corresponding reference values. During the TR event, the mean values differ from the reference plots, specifically the onset, rate and maximum temperature of TR. This difference is due to the TR event occurring at different times in each simulation run. Therefore, where the peak temperature occurs for the reference simulation, for other simulations at this point in time the temperature may be significantly lower as TR may not have started yet. This causes the overall mean temperature to have a lower maximum and shallower gradient during the TR event, rather than following a steep increase in temperature that is present in each individual simulation. Also, by looking at the STD, we can see that it increases significantly during the TR period, whilst in general the STD is greater for steeper temperature rates. This increase in STD causes a sudden drop in the lower bound of the data, even though for any of the 753 runs, a decrease in temperature similar to the dip in the lower bound is not possible.

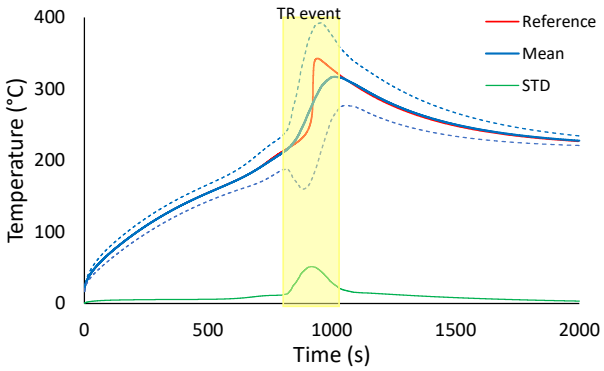

Figure 3: Mean results of all 753 oven simulations, each with randomly sampled thermo-physical characteristics, and compared to the reference simulation.

3.2. Time-Dependent Temperature Analysis

3.2.1. GP Validation

The GP surrogate was used to predict the temperature at given times using the five thermo-physical and heat transfer characteristics as inputs to the GP. Therefore, $10s$ time steps were used up to the TR event and then, to capture the process accurately $2s$ time steps were used between $800s$ and $1200s$. Hence, the GP surrogate model consisted of 361 independent GPs, predicting the temperature at each time step. To be able to confidently calculate the Sobol' indices using a surrogate model the predictions produced by the GPs must be fully validated against the

oven simulations to ensure inaccuracies are not inherently produced in the GSA. For this reason, the GP surrogate model was tested using the 5-fold cross-validation technique (Hastie, 2009) and the final results are as follows:

- Figure 4a presents the residuals, a comparison of the true values with the predicted mean values for each test prediction. A "high" predictive quality is indicated by the data following closely to the red $y = x$ trend line and a high coefficient of determination value of 0.969 (Marrel et al., 2008; Rohmer and Foerster, 2011).

- Figure 4b shows the test predictions as a function of time by considering the root mean squared error indicating the predictions have negligible errors up to and after the TR event. Between $850s$ and $1150s$, the RMSE increases to a maximum of 0.400.

- Figure 4c considers the predictive distribution by looking at the percentage of outliers at 2 STD's with respect to time. These outliers include any test prediction where it's true standardised value is outside of the predictions 95% uncertainty distribution. Again, before and after the TR event the number of outliers is negligible but during the TR event the percentage of outliers increase to be between 4% and 12%. Figure 4c also shows the percentage of predictions where the true test value is further than 4 predictive STD's away from the predicted mean.

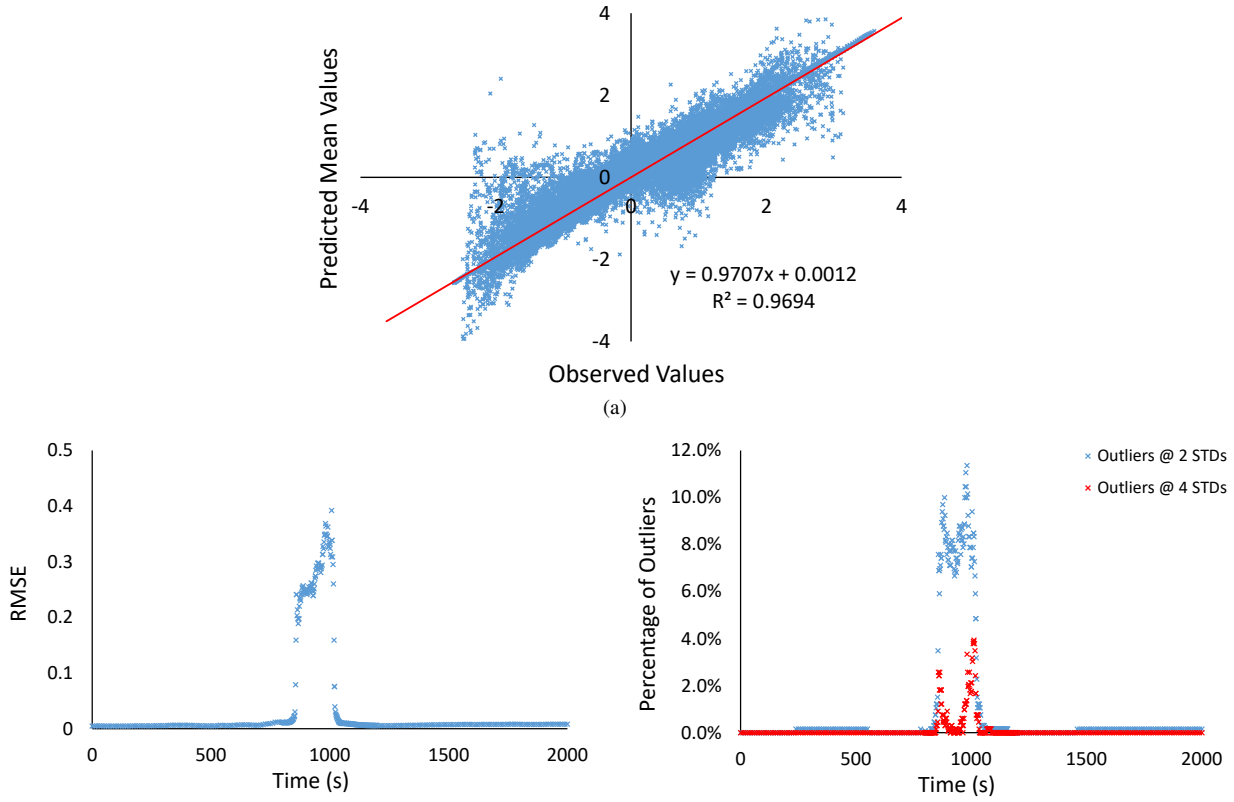

(a)

(b)

(c)

Figure 4: The diagnostics comparing the true standardised temperature to the standardised test predictions used to validate the time-dependent GPs using 5-fold cross-validation: a) the residuals b) the RMSE, c) the outliers.

Figure 5 shows the variation in temperature with time as predicted by the GP surrogate model using the mean input values. The temperature-time profile allows a direct comparison of the reference oven simulation to the predicted distribution which includes the mean predicted temperature (shown by the solid blue line) and the 95% confidence limits (shown by the dashed blue lines). At first, the accuracy of the GP is clear to see as the blue line closely follows the red reference line. Additionally, the uncertainty in the predictions is very small shown by the 95% confidence limits being barely distinguishable lines.

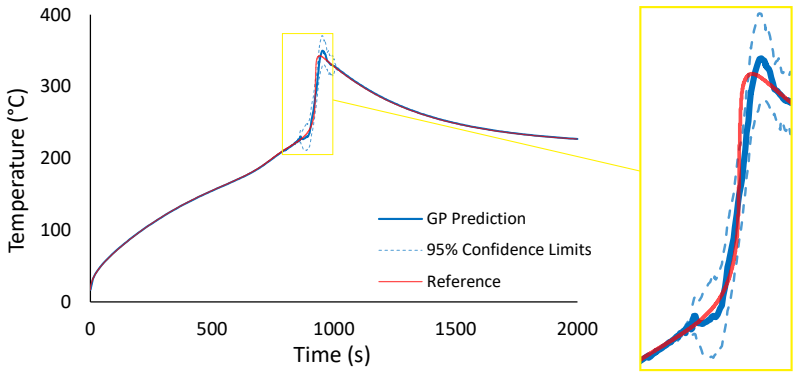

Figure 5: The predicted temperature-time profile from the GPs when the inputs are kept constant at the mean values.

Overall, the test predictions have been analysed in detail by comparing the residuals, the diagnostics as a function of time and by fitting a GP to compare with the reference model. This has made it clear to see the predictions using the GP surrogate model are satisfactory and so we can confidently calculate the Sobol' indices.

3.2.2. Sobol' Indices

The Sobol' indices for each of the five inputs as a function of time, resulting from the GSA, are presented in Figure 6. Also shown in the figure is the mean temperature which allows us to study the dynamics of the system. Figure 6a shows the first-order Sobol' indices, including the interactions between all the inputs. Figure 6b shows the total Sobol' indices for each input. As can be seen in both figures, the surface temperature is first dominated by the conductivity coefficient. Hence, during the first instances of the cell being heated externally, it is the cells' ability to transfer heat to the bulk of the mass that has the most dominant effects on surface temperature. In other words, a higher/ lower conductivity coefficient will mean that heat from the cells surface can be more/ less easily transferred through the cell to the bulk, leading to relatively lower/ higher surface temperatures, respectively.

From the beginning of the oven simulation to $500s$ the cells' temperature increases and so does the sensitivity measure of the emissivity and convection coefficient increase, with a corresponding decrease in the sensitivity measure of the conductivity coefficient. At $120s$ the sum of the sensitivity measures of the emissivity and convection coefficient equal that of the conductivity. Hence, at this temperature, we can say that the total heat exchange from the environment is the most important factor in cell temperature prediction. Beyond this time, the Sobol' indices of the emissivity coefficient continues to increase with further reduction in the Sobol' indices of the conductivity coefficient, while the Sobol' indices of the convection coefficient remain relatively constant. At $130s$ the emissivity becomes the most dominant factor in the overall uncertainty in cell temperature predictions, continuing up until the TR event reaching a maximum of 79.6% of the total output variance at $580s$.

Between $600s$ and $800s$, it can be seen from Figure 6a that the Sobol' indices of the conductivity coefficient

increases. When comparing this to the temperature plot in the same graph, it can be seen that this corresponds to an increase in the slope of the temperature. The increase in the slope of the temperature is attributed to the increase in self-heating, as all else remains constant. Hence, the greater importance of the value of thermal conductivity shows the governing heat transfer to be the transfer of the decomposition heat from the jelly roll to the surface.

It can clearly be seen in Figure 6a that before $800s$, i.e. the start of TR, interactions between inputs are not involved in the process. Whereas, between $800s$ and $1100s$, we can see from Figure 6a that the interactions have a much larger effect on the output temperature. From Figure 6b we can see that these noticeable interactions must be between the heat capacity, conductivity coefficient, convection coefficient and emissivity, as the Sobol' indices of these inputs increase by a large amount from first-order Sobol' indices to total Sobol' indices. When the majority of the oven simulations have reached the peak of TR at around $1050s$ (as shown by the mean temperature of the data) it can be seen that the total Sobol' indices of emissivity are large, almost reaching 1. However, at this same stage the first-order Sobol' indices of emissivity are below 0.3, showing that emissivity's interactions have a large effect on the output temperature when the TR event is reaching its finale. An increase from first order Sobol' indices to the total Sobol' indices for the conductivity coefficient and the convective coefficient show that the interactions must be between emissivity and these two thermal properties. Whereas, in comparison, the heat capacity and the density have a small increase in Sobol' values from first order to total. Hence, additional to the need to characterise emissivity well, as mentioned previously, it is shown that the convection coefficient and conductivity coefficient need also be characterised well to enable confident predictions of the TR event. Whereas, the results indicate that the density and heat capacity value could be estimated, knowing confidently that the values should have zero effect on the outcome of the oven simulation.

As shall be discussed in Section 4, calculating Sobol' indices for dependent inputs may create inaccuracies in the results as the method relies on independent variables Mara and Tarantola (2012). In spite of this, as the calculated Sobol' indices for both density and heat capacity are very small, we can assume that this is negligible.

Another important consideration is the high confidence in the experimental results which could cause the Sobol' indices for the density input variable to be small. This level of confidence in experiments has caused the relative standard deviation (RSTD) of density to be much smaller than the other input variables and so the variability of the density in the oven simulations is much smaller. This, along with the fact that the RSTD of density is less than a quarter to the RSTD of its dependent variable, the heat capacity, ensures that the small changes in density do not affect the output of the simulations. It should also be noted that the confidence of the heat capacity is relatively high. However, reported values in the literature between 18650 cells for the heat capacity vary greatly, and hence would increase the variance in the results if the C_p had a STD that encompassed the literature range of values.

Once TR has completed and the battery begins to cool, the variation in the Sobol' indices decreases as the cross effects become negligible. After this period the battery cools towards the oven temperature and so the relevance of emissivity and the convection coefficient begin to slowly reduce linearly. Whereas, the conductivity coefficient starts to increase again, due to the dominant heat transfer from inside the cell to its surface and the environment, from almost zero relevance straight after the TR event to joining the convection coefficient's value of Sobol' indices. Nonetheless, it is clear that the most dominant thermo-physical and heat transfer characteristic is the emissivity, reducing from 0.81 at the time the TR event is over to 0.77 to the time the oven simulation has finished at $2000s$. In agreement with this result, the importance of radiation in TR of Li-ion cells has has also been shown experimentally (Hatchard et al., 2000; Chen et al., 2006).

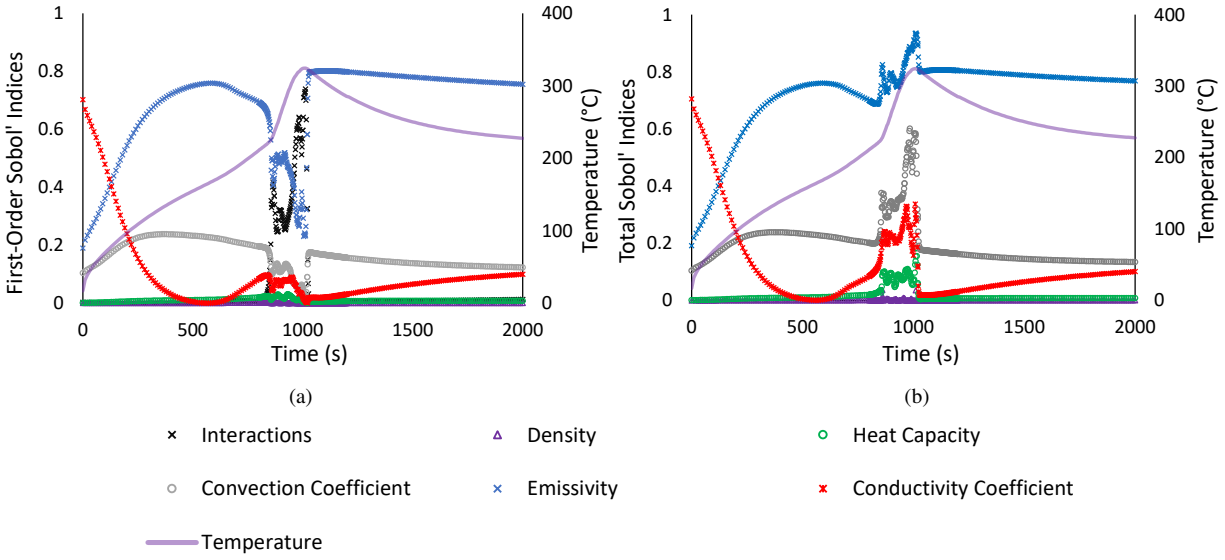

Figure 6: The Sobol' indices for each input as a function of time: a) shows the first-order Sobol' indices and the interactions, b) shows the total Sobol' indices.

3.3. TR Features Analysis

3.3.1. GP Validation

The time-dependent data showed emissivity to be the most dominant thermo-physical and heat transfer characteristic throughout the oven simulation, nevertheless, it is important to understand how this effects the key steps in a TR event. Consequently, after looking at the time-series data, the research shall now build on this knowledge, further understanding how the input variables have an impact on the three important TR features.

The time-dependent data showed emissivity to be the most dominant thermo-physical and heat transfer characteristic throughout the oven simulation furthering our understanding of the TR modelling process. Additionally, a

similar analysis was used to assist the time-series analysis, to consider how the input variables have an impact on three important TR features. We therefore perform a further GSA on the following features:

- Self-heating onset - defined as the point in time at which self-heating becomes dominant. Calculated as the time at which the rate of change in temperature goes from a negative slope to a positive slope, i.e the inflection point of temperature rate, marked "IP" on the temperature rate plot of Figure 2.
- TR onset time - the time at which the TR event begins. It is defined and calculated as the time at which the temperature rate goes above $1°Cs^{-1}$ after the initial 500 seconds of heating, marked "TR" on the temperature rate plot of Figure 2
- Maximum temperature - marked as "T_{max}" on Figure 2.

Once again, a 5-fold cross validation of the GP outputs were performed just as before enabling a plot of the residuals shown in Figure 4a, comparing the observed values to the predicted mean values show the three GPs to have an excellent predictive quality, achieving a coefficient of determination value of 0.9998. Additionally, Table 4 shows the three outputs individually have low values close to zero for the outliers at 2 STD's and the RMSE.

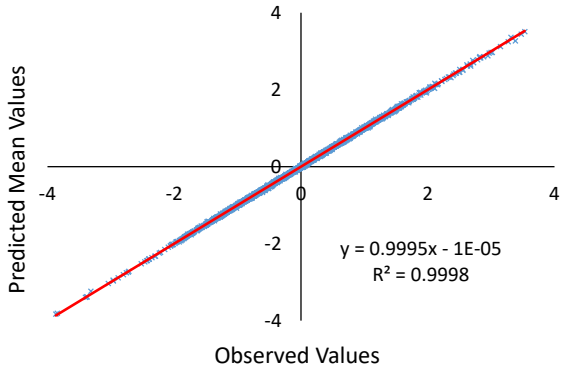

Figure 7: The residuals showing the observed standardised values against the predicted standardised values for all of the oven simulation test predictions.

Table 4: Resulting diagnostic values from the time prediction GPs

Output	**Outliers at 2 STD's**	**RMSE**
Inflection Point	0.266%	0.0225
TR Onset Time	0.133%	0.00763
Maximum Temperature	0.000%	0.00607

3.3.2. Sobol' Indices

The SA of the three important TR conditions were conducted to find which of the thermo-physical and heat transfer characteristics had the greatest effects on the time and severity of TR. The results are the total Sobol' indices calculated for each output can be seen in Figure 8 where the bars are split between the first-order and cross effects for the three different outputs. Figure 8a and Figure 8b clearly show the emissivity to be the most relevant thermo-physical and heat transfer characteristic for the important times dictating the TR event. Another interesting feature shown through the first two bar charts is that as the cell is first heated up to the inflection point, conductivity has little effect on the speed of the process. Although, for the TR onset time the total Sobol' indices for conductivity increases slightly. This infers that once self-heating of the battery becomes dominant (the inflection point) then conductivity has an increased effect on the TR. Once again, density and heat capacity have very little relevance on the output of the times during the TR process. Whereas, the TR severity has found the calculated Sobol' indices to show different relevance of importance for the input variables to all the previous results. The TR severity is described by the maximum temperature reached in the TR event and the total Sobol' indices calculated are shown in Figure 8c stating that the conductivity coefficient is the most dominant input, followed by the heat capacity and then the emissivity. In this case, both the density and the convection coefficient have no effect on the maximum temperature reached by the oven simulation. This shows the complexity involved in parametrising a TR model for Li-ion cells considering the whole process has previously shown to be dominated by the emissivity, it has now been shown that severity is dominated by a mixture of the three inputs. These results concur with the previous time-dependent Sobol' indices as the figures show very little red bars proving the interactions between inputs have small relevance leading up the TR events.

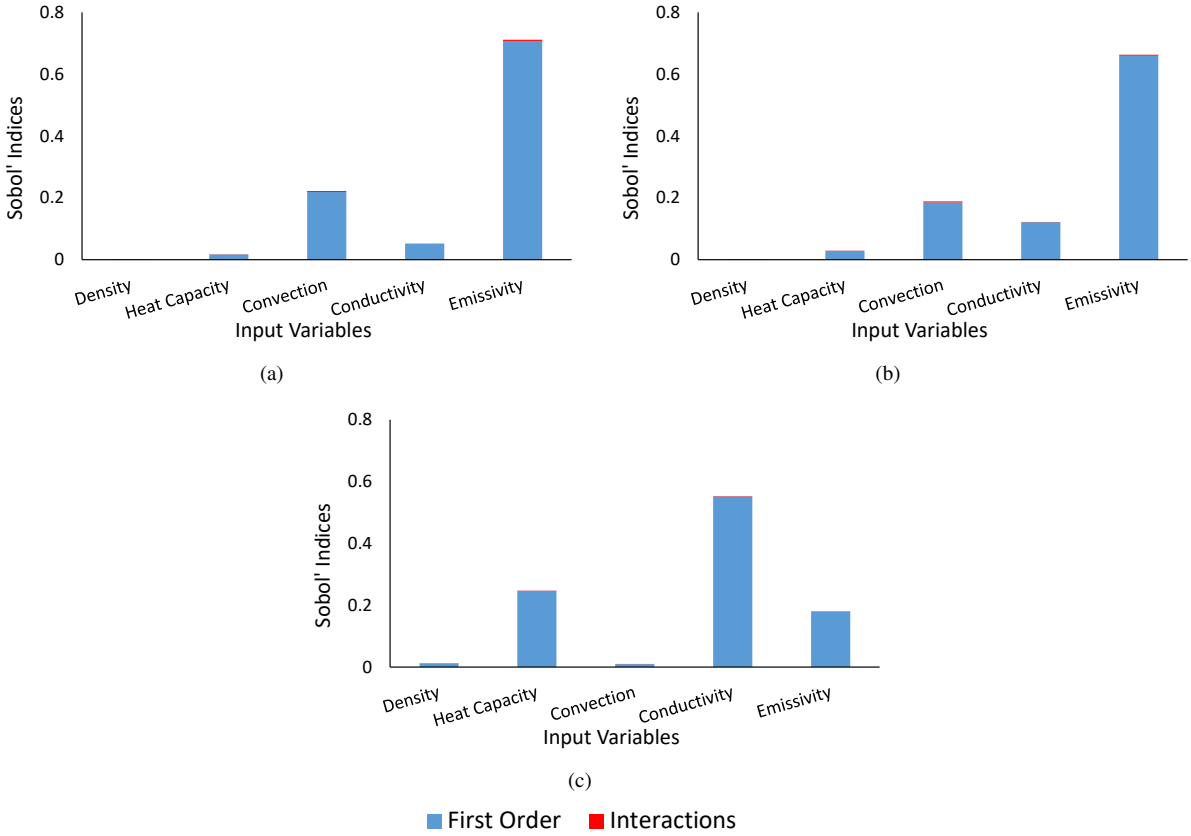

Figure 8: The total Sobol' indices for each input split to show the interactions and the first order Sobol' indices for each output: a) inflection point, b) TR onset time, and c) maximum temperature during TR.

To summarise, the SA outlines the importance of the values chosen for the development of TR models. It can be seen that estimating the emissivity value would not be adequate for a model as the sensitivity indices have shown that this dominates the whole TR process. Therefore, the SA has proven important in relation to Li-ion cell TR by providing vital information on the thermo-physical and heat transfer characteristics in respect to their effects on the temperature. From that, the research has also discovered that leading up to TR events the most dominant property is, again, emissivity as the inflection point and the TR onset time is considered. Although, when considering the severity of the TR event, analysing the maximum temperature reached by the oven simulations has found that the conductivity coefficient is the most dominant input. Additionally, heat capacity has zero impact on when TR occurs but it does have a say in the maximum temperature as the Sobol' indices for heat capacity increase with respect to the maximum temperature.

4. Conclusion

Modelling the thermal runaway (TR) of Li-ion cells is intrinsically as important as it is difficult due to the lack of understanding in the model parameters. A large number of parameters that govern the rise in temperature of a cell ensure the accuracy of simulation models difficult to obtain. Therefore, further understanding of some of the many properties was analysed in this research. Beginning with a GSA of the thermo-physical and heat transfer characteristics of a Li-ion cell provides guidelines into which parameters are the most important when designing the TR model. This was achieved by developing a TR abuse model for an LFP cell case study whereby all the parameters except the thermo-physical and heat transfer properties were kept constant to generate enough simulations for a variance-based GSA. With the use of a GP surrogate model, the Sobol' indices of the five inputs were calculated. Consequently, care was taken to validate the surrogate model ensuring inaccuracies were not carried onto the GSA.

The calculated Sobol' indices found that the most dominant parameter through the overall abuse scenario is clearly the emissivity value. This statement is true when considering the time-dependent Sobol' indices throughout the TR process as well as the Sobol' indices when considering the two key time points as an output. However, when the severity of the TR event is considered, emissivity is no longer the dominant variable and now the conductivity coefficient has a much larger Sobol' indices. Hence, Li-ion safety will benefit by ensuring the radiation is controlled with care and when designing a TR model it is essential the emissivity is well characterised to avoid uncertainty in the model output. We have shown which parameters are key and at what point during TR, enabling other researchers to interpret their results better given their confidence in parameter values. The work carried out should ensure more accurate and robust TR models are developed by showing the important parameters to obtain. This further benefits the energy storage community as these uncertainties in the TR models are related to physical cells and so the relevant phenomena to consider for Li-ion safety are known.

As this model does not account of axial conductivity, which could lead to a greater temperature rate of the cell from increased heat transfer from the oven, reaction parameters may have to be altered to ensure accurate TR predictions. However, as the overall TR behaviour would be similar in any instance, one can assume the general dependences (of TR on parameters) would be similar. This is with the exception that the conductivity coefficient in the axial direction would have a greater influence on the model than the value in the radial direction. The GP SA techniques used here can be readily applied to higher dimensional models that include this extra heat transfer path but this is beyond the scope of this work.

For future work this study will be extended to the parameters governing the reaction kinetics and decomposition heat within the TR model, further developing the work begun by Milton et al. (2019) by understanding the effects each parameter has on the output. The GP model will be improved so that the uncertainty in predictions cover a wider range

allowing a wider range of oven simulations to be used. Particularly, care will be taken in predictions for TR events that occur incredibly early/late so that the GP can successfully predict temperatures up to 10 STD's away from the mean at these early/late times. Another important aspect to consider is the range of input variables as this work gleaned the range of values from experimental work but an increase of 10% would reflect a larger variation of parameter values quoted in the literature. Furthermore, an unpublished analysis of the full order oven simulation has shown that a 10% increase/decrease in heat capacity has a large effect on the resulting temperature-time graph. Whereas this research has shown that the range of heat capacity found from experimental work has very little significance on the resulting temperature profile. On a more practical level, it would be beneficial to consider the effects of all the model parameters together and apply the method for various other battery chemistries.

References

Abada, S., Marlair, G., Lecocq, A., Petit, M., Sauvant-Moynot, V., Huet, F., 2016. Safety focused modeling of lithium-ion batteries: A review. Journal of Power Sources 306, 178–192. doi:10.1016/j.jpowsour.2015.11.100.

Al, R., Behera, C.R., Zubov, A., Gernaey, K.V., Sin, G., 2019. Meta-modeling based efficient global sensitivity analysis for wastewater treatment plants – An application to the BSM2 model. Computers & Chemical Engineering 127, 233–246. URL: https://doi.org/10.1016/j.compchemeng.2019.05.015, doi:10.1016/j.compchemeng.2019.05.015.

Brown, S., Beck, J., Mahgerefteh, H., Fraga, E.S., 2013. Global sensitivity analysis of the impact of impurities on CO2 pipeline failure. Reliability Engineering and System Safety 115, 43–54. URL: http://dx.doi.org/10.1016/j.ress.2013.02.006, doi:10.1016/j.ress.2013.02.006.

Bugryniec, P.J., Davidson, J.N., Brown, S.F., 2018. Assessment of thermal runaway in commercial lithium iron phosphate cells due to over-heating in an oven test. Energy Procedia 151, 74–78. URL: https://doi.org/10.1016/j.egypro.2018.09.030, doi:10.1016/j.egypro.2018.09.030.

Bugryniec, P.J., Davidson, J.N., Cumming, D.J., Brown, S.F., 2019. Pursuing safer batteries: Thermal abuse of LiFePO4 cells. Journal of Power Sources 414, 557–568. doi:10.1016/j.jpowsour.2019.01.013.

Chen, S., Wan, C., Wang, Y., 2005a. Thermal analysis of lithium-ion batteries. Journal of Power Sources 140, 111 – 124. URL: http://www.sciencedirect.com/science/article/pii/S0378775304008596, doi:https://doi.org/10.1016/j.jpowsour.2004.05.064.

Chen, S.C., Wang, Y.Y., Wan, C.C., 2006. Thermal Analysis of Spirally Wound Lithium Batteries. Journal of The Electrochemical Society 153, A637. doi:10.1149/1.2168051.

Chen, W., Jin, R., Sudjianto, A., 2005b. Analytical Variance-Based Global Sensitivity Analysis in Simulation-Based Design Under Uncertainty. Journal of Mechanical Design 127, 875. doi:10.1115/1.1904642.

Chiu, K.C., Lin, C.H., Yeh, S.F., Lin, Y.H., Chen, K.C., 2014. An electrochemical modeling of lithium-ion battery nail penetration. Journal of Power Sources 251, 254–263. URL: http://dx.doi.org/10.1016/j.jpowsour.2013.11.069, doi:10.1016/j.jpowsour.2013.11.069.

Coleman, B., Ostanek, J., Heinzel, J., 2016. Reducing cell-to-cell spacing for large-format lithium ion battery modules with aluminum or PCM heat sinks under failure conditions. Applied Energy 180, 14–26. URL: http://dx.doi.org/10.1016/j.apenergy.2016.07.094, doi:10.1016/j.apenergy.2016.07.094.

Coman, P.T., Darcy, E.C., Veje, C.T., White, R.E., 2017. Modelling Li-Ion Cell Thermal Runaway Triggered by an Internal Short Circuit

Device Using an Efficiency Factor and Arrhenius Formulations. Journal of The Electrochemical Society 164, A587–A593. doi:10.1149/2.0341704jes.

COMSOL Multiphysics®V5.2a, . www.comsol.com. COMSOL AB, Stockholm, Sweden.

Dong, T., Peng, P., Jiang, F., 2018. Numerical modeling and analysis of the thermal behavior of NCM lithium-ion batteries subjected to very high C-rate discharge/charge operations. International Journal of Heat and Mass Transfer 117, 261–272. URL: https://doi.org/10.1016/j.ijheatmasstransfer.2017.10.024, doi:10.1016/j.ijheatmasstransfer.2017.10.024.

Drake, S., Wetz, D., Ostanek, J., Miller, S., Heinzel, J., Jain, A., 2014. Measurement of anisotropic thermophysical properties of cylindrical li-ion cells. Journal of Power Sources 252, 298 – 304. URL: http://www.sciencedirect.com/science/article/pii/S0378775313019502, doi:https://doi.org/10.1016/j.jpowsour.2013.11.107.

Drews, T.O., Braatz, R.D., Alkire, R.C., 2003. Parameter Sensitivity Analysis of Monte Carlo Simulations of Copper Electrodeposition with Multiple Additives. Journal of The Electrochemical Society 150, C807. doi:10.1149/1.1617305.

Duan, X., Jiang, W., Zou, Y., Lei, W., Ma, Z., 2018. A coupled electrochemical–thermal–mechanical model for spiral-wound Li-ion batteries. Journal of Materials Science 53, 10987–11001. URL: https://doi.org/10.1007/s10853-018-2365-6, doi:10.1007/s10853-018-2365-6.

Feng, X., Ouyang, M., Liu, X., Lu, L., Xia, Y., He, X., 2018. Thermal runaway mechanism of lithium ion battery for electric vehicles: A review. Energy Storage Materials 10, 246 – 267. URL: http://www.sciencedirect.com/science/article/pii/S2405829716303464, doi:https://doi.org/10.1016/j.ensm.2017.05.013.

Ghadbeigi, L., Harada, J.K., Lettiere, B.R., Sparks, T.D., 2015. Performance and resource considerations of li-ion battery electrode materials. Energy Environ. Sci. 8, 1640–1650. URL: http://dx.doi.org/10.1039/C5EE00685F, doi:10.1039/C5EE00685F.

Guo, G., Long, B., Cheng, B., Zhou, S., Xu, P., Cao, B., 2010. Three-dimensional thermal finite element modelling of lithium-ion battery in thermal abuse application. Journal of Power Sources 195, 2393–2398. doi:10.1016/j.jpowsour.2009.10.090.

Hastie, T., 2009. The elements of statistical learning : data mining, inference, and prediction. Springer series in statistics. 2nd ed. ed., Springer, New York.

Hatchard, T.D., MacNeil, D.D., Basu, A., Dahn, J.R., 2001. Thermal Model of Cylindrical and Prismatic Lithium-Ion Cells. Journal of The Electrochemical Society 148, A755–A761. doi:10.1149/1.1377592.

Hatchard, T.D., Macneil, D.D., Stevens, D.A., Christensen, L., Dahn, J.R., 2000. Importance of Heat Transfer by Radiation in Li-Ion Batteries during Thermal Abuse. Electrochemical and Solid-Stae Letters 3, 305–308.

Hu, B., Ma, Z., Lei, W., Zou, Y., Lu, C., 2017. A chemo-mechanical model coupled with thermal effect on the hollow core–shell electrodes in lithium-ion batteries. Theoretical and Applied Mechanics Letters 7, 199–206. URL: http://dx.doi.org/10.1016/j.taml.2017.09.001, doi:10.1016/j.taml.2017.09.001.

International Energy Agency, 2016. Global EV Outlook 2016: Beyond one million electric cars. Technical Report. Paris. URL: Availableat: https://www.iea.org/publications/freepublications/publication/Global_EV_Outlook_2016.pdf. [accessed 2 August 2016].

Jiang, J., Dahn, J.R., 2004. ARC studies of the thermal stability of three different cathode materials: $LiCoO_2$; $Li[Ni_{0.1}Co_{0.8}Mn_{0.1}]O_2$; and $LiFePO_4$, in $LiPF_6$ and LiBoB EC/DEC electrolytes. Electrochemistry Communications 6, 39–43. doi:10.1016/j.elecom.2003.10.011.

Jin, R., Chen, W., Sudjianto, A., 2004. Analytical metamodel-based global sensitivity analysis and uncertainty propagation for robust design. SAE Transactions Journal of Materials & Manufacturing doi:10.4271/2004-01-0429.

Kim, G.H., Pesaran, A., Spotnitz, R., 2007. A three-dimensional thermal abuse model for lithium-ion cells. Journal of Power Sources 170, 476–489. doi:10.1016/j.jpowsour.2007.04.018.

Kim, T.H., Park, J.S., Chang, S.K., Choi, S., Ryu, J.H., Song, H.K., 2012. The Current Move of Lithium Ion Batteries Towards the Next Phase. Advanced Energy Materials 2, 860–872. doi:10.1002/aenm.201200028.

Larsson, F., Bertilsson, S., Furlani, M., Albinsson, I., Mellander, B.E., 2018. Gas explosions and thermal runaways during external heating abuse of commercial lithium-ion graphite-LiCoO2 cells at different levels of ageing. Journal of Power Sources 373, 220 – 231. URL: http://www.sciencedirect.com/science/article/pii/S0378775317314398, doi:https://doi.org/10.1016/j.jpowsour.2017.10.085.

Li, S., Yang, B., Qi, F., 2016. Accelerate global sensitivity analysis using artificial neural network algorithm: Case studies for combustion kinetic model. Combustion and Flame 168, 53–64. doi:10.1016/j.combustflame.2016.03.028.

Lin, N., Xie, X., Schenkendorf, R., Krewer, U., 2018. Efficient Global Sensitivity Analysis of 3D Multiphysics Model for Li-Ion Batteries. Journal of Electrochemical Society 165, A1169–A1183. doi:10.1149/2.1301805jes.

Liu, X., Wu, Z., Stoliarov, S.I., Denlinger, M., Masias, A., Snyder, K., 2018. A Thermo-Kinetic Model of Thermally-Induced Failure of a Lithium Ion Battery: Development, Validation and Application. Journal of Electroanalytical Society 165, A2909–A2918. doi:10.1149/2.0111813jes.

Lopez, C.F., Jeevarajan, J.A., Mukherjee, P.P., 2015. Characterization of Lithium-Ion Battery Thermal Abuse Behavior Using Experimental and Computational Analysis. Journal of The Electrochemical Society 162, A2163–A2173. doi:10.1149/2.0751510jes.

Ma, Z., Wu, H., Wang, Y., Pan, Y., Lu, C., 2017. An electrochemical-irradiated plasticity model for metallic electrodes in lithium-ion batteries. International Journal of Plasticity doi:10.1016/j.ijplas.2016.10.009.

MacNeil, D.D., Christensen, L., Landucci, J., Paulsen, J.M., Dahn, J.R., 2000. An Autocatalytic Mechanism for the Reaction of Li_xCoO_2 in Electrolyte at Elevated Temperature. Journal of The Electrochemical Society 147, 970–979. doi:10.1149/1.1393299.

Mao, B., Huang, P., Chen, H., Wang, Q., Sun, J., 2020. Self-heating reaction and thermal runaway criticality of the lithium ion battery. International Journal of Heat and Mass Transfer doi:10.1016/j.ijheatmasstransfer.2019.119178.

Mara, T.A., Tarantola, S., 2012. Variance-based sensitivity indices for models with dependent inputs. Reliability Engineering and System Safety 107, 115–121. URL: http://dx.doi.org/10.1016/j.ress.2011.08.008, doi:10.1016/j.ress.2011.08.008.

Marrel, A., Iooss, B., Laurent, B., Roustant, O., 2009. Calculations of Sobol indices for the Gaussian process metamodel. Reliability Engineering and System Safety 94, 742–751. doi:10.1016/j.ress.2008.07.008.

Marrel, A., Iooss, B., Van Dorpe, F., Volkova, E., 2008. An efficient methodology for modeling complex computer codes with Gaussian processes. Computational Statistics and Data Analysis 52, 4731–4744. doi:10.1016/j.csda.2008.03.026, arXiv:0802.1099.

Milton, R., Bugryniec, P., Brown, S., 2019. Parameter estimation for thermal runaway of li-ion cells: a gaussian process approach, in: Kiss, A.A., Zondervan, E., Lakerveld, R., Özkan, L. (Eds.), 29th European Symposium on Computer Aided Process Engineering. Elsevier. volume 46 of *Computer Aided Chemical Engineering*, pp. 775 – 780. URL: http://www.sciencedirect.com/science/article/pii/B9780128186343501302, doi:https://doi.org/10.1016/B978-0-12-818634-3.50130-2.

Nitta, N., Wu, F., Lee, J.T., Yushin, G., 2015. Li-ion battery materials: present and future. Materials Today 18, 252 – 264. URL: http://www.sciencedirect.com/science/article/pii/S1369702114004118, doi:https://doi.org/10.1016/j.mattod.2014.10.040.

Peng, P., Jiang, F., 2016. Thermal safety of lithium-ion batteries with various cathode materials: A numerical study. International Journal of Heat and Mass Transfer 103, 1008–1016. doi:10.1016/j.ijheatmasstransfer.2016.07.088.

Peters, J.F., Baumann, M., Zimmermann, B., Braun, J., Weil, M., 2017. The environmental impact of li-ion batteries and the role of key parameters – a review. Renewable and Sustainable Energy Reviews 67, 491 – 506. URL: http://www.sciencedirect.com/science/article/pii/S1364032116304713, doi:https://doi.org/10.1016/j.rser.2016.08.039.

Rajan, A., Vijayaraghavan, V., Ooi, M.P.L., Garg, A., Kuang, Y.C., 2018. A simulation-based probabilistic framework for lithium-ion battery modelling. Measurement: Journal of the International Measurement Confederation 115, 87–94. URL: http://dx.doi.org/10.1016/j.measurement.2017.10.033, doi:10.1016/j.measurement.2017.10.033.

Ren, D., Liu, X., Feng, X., Lu, L., Ouyang, M., Li, J., He, X., 2018. Model-based thermal runaway prediction of lithium-ion batteries from kinetics analysis of cell components. Applied Energy 228, 633–644. URL: https://doi.org/10.1016/j.apenergy.2018.06.126, doi:10.1016/j.apenergy.2018.06.126.

Richard, M.N., Dahn, J.R., 1999a. Accelerating Rate Calorimetry Study on the Thermal Stability of Lithium Intercalated Graphite in Electrolyte I. Experimental. Journal of The Electrochemical Society 146, 2068–2077. doi:10.1149/1.1391894.

Richard, M.N., Dahn, J.R., 1999b. Accelerating Rate Calorimetry Study on the Thermal Stability of Lithium Intercalated Graphite in Electrolyte. II. Modeling the Results and Predicting Differential Scanning Calorimeter Curves. Journal of The Electrochemical Society 146, 2078–2084. doi:10.1149/1.1391894.

Rohmer, J., Foerster, E., 2011. Global sensitivity analysis of large-scale numerical landslide models based on Gaussian-Process meta-modeling. Computers and Geosciences 37, 917–927. URL: http://dx.doi.org/10.1016/j.cageo.2011.02.020, doi:10.1016/j.cageo.2011.02.020.

ROMCOMMA, 2019. https://github.com/C-O-M-M-A/rom-comma. [Online]. [Accessed on 25 November 2019].

Saltelli, A., Homma, T., 1996. Importance measures in global sensitivity analysis of model output. Reliab. Eng. Sys. Safety 52, 1–17.

Saltelli, A., Ratto, M., Tarantola, S., Campolongo, F., 2005. Sensitivity Analysis for Chemical Models. Chemical Reviews 105, 2811–2828. URL: https://pubs.acs.org/doi/10.1021/cr040659d, doi:10.1021/cr040659d.

Schmidt, A.P., Bitzer, M., Imre, Á.W., Guzzella, L., 2010. Experiment-driven electrochemical modeling and systematic parameterization for a lithium-ion battery cell. Journal of Power Sources 195, 5071–5080. doi:10.1016/j.jpowsour.2010.02.029.

Shack, P., Iannello, C., Rickman, S., Button, R., 2014. NASA Perspective and Modeling of Thermal Runaway Propagation Mitigation in Aerospace Batteries.

Sobol, I.M., 1993. Sensitivity analysis for nonlinear mathematical models. Mathematical Modelling Computational Experiments 1, 407–414. URL: http://max2.ese.u-psud.fr/epc/conservation/MODE/SobolOriginalPaper.pdf{%}0Ahttp://www.mathnet.ru/eng/mm2320, doi:10.18287/0134-2452-2015-39-4-459-461., arXiv:arXiv:1305.4373v1.

Sobol, I.M., 2001. Global sensitivity indices for nonlinear mathematical models. Review. Mathematics and Computers in Simulation , 271–280.

Spinner, N.S., Mazurick, R., Brandon, A., Rose-pehrsson, S.L., Tuttle, S.G., 2015. Analytical, Numerical and Experimental Determination of Thermophysical Properties of Commercial 18650 LiCoO 2 Lithium-Ion Battery. Journal of The Electrochemical Society 162, A2789–A2795. doi:10.1149/2.0871514jes.

Spotnitz, R., Franklin, J., 2003. Abuse behavior of high-power, lithium-ion cells. Journal of Power Sources 113, 81–100.

Steen, M., Lebedeva, N., Di Persio, F., Boon-Brett, L., 2017. EU Competitiveness in Advanced Li-ion Batteries for E-Mobility and Stationary Storage Applications – Opportunities and Actions. Technical Report. European Commission's Joint Research Centre. URL: http://publications.jrc.ec.europa.eu/repository/bitstream/JRC108043/kjna28837enn.pdf. [accessed 1 September 2018].

Stein, M., 1987. Large sample properties of simulations using Latin hypercube sampling. Technometrics 29, 143–151. URL: http://www.jstor.org/stable/10.2307/1269769.

Sudret, B., 2008. Global sensitivity analysis using polynomial chaos expansions. Reliability Engineering and System Safety 93, 964–979. doi:10.1016/j.ress.2007.04.002.

Tanaka, N., Bessler, W.G., 2014. Numerical investigation of kinetic mechanism for runaway thermo-electrochemistry in lithium-ion cells. Solid State Ionics 262, 70–73. URL: http://dx.doi.org/10.1016/j.ssi.2013.10.009, doi:10.1016/j.ssi.2013.10.009.

Trembacki, B., Harris, S.R., Piekos, E.S., Roberts, S.A., 2016. Uncertainty Quantification, Verification, and Validation of a Thermal Simulation Tool for Molten Salt Batteries, in: 47th Power Sources Conference, Sandia National Lab. (SNL-NM), Albuquerque, NM (United States). URL: https://www.osti.gov/servlets/purl/1365182.

Vazquez-Arenas, J., Gimenez, L.E., Fowler, M., Han, T., Chen, S.K., 2014. A rapid estimation and sensitivity analysis of parameters describing the behavior of commercial Li-ion batteries including thermal analysis. Energy Conversion and Management 87, 472–482. URL: http://dx.doi.org/10.1016/j.enconman.2014.06.076, doi:10.1016/j.enconman.2014.06.076.

Wang, Q., Ping, P., Zhao, X., Chu, G., Sun, J., Chen, C., 2012. Thermal runaway caused fire and explosion of lithium ion battery. Journal of Power Sources 208, 210–224. doi:10.1016/j.jpowsour.2012.02.038.

Wang, S., Lu, L., Liu, X., 2013. A simulation on safety of $LiFePO_4$/C cell using electrochemical-thermal coupling model. Journal of Power Sources 244, 101–108. doi:10.1016/j.jpowsour.2013.03.100.

Wipf, D.P., Nagarajan, S., 2007. A New View of Automatic Relevance Determination, in: Proceedings of the 20th International Conference on Neural Information Processing Systems, NIPS'07, Curran Associates Inc.. pp. 1625–1632. URL: http://citeseerx.ist.psu.edu/viewdoc/download?doi=10.1.1.143.8009{&}rep=rep1{&}type=pdf.

Wu, H., Xie, Z., Wang, Y., Zhang, P., Sun, L., Lu, C., Ma, Z., 2019. A constitutive model coupling irradiation with two-phase lithiation for lithium-ion battery electrodes. Philosophical Magazine 99, 992–1013. doi:10.1080/14786435.2019.1569767.

Xu, J., Lan, C., Qiao, Y., Ma, Y., 2017. Prevent thermal runaway of lithium-ion batteries with minichannel cooling. Applied Thermal Engineering 110, 883–890. URL: http://dx.doi.org/10.1016/j.applthermaleng.2016.08.151, doi:10.1016/j.applthermaleng.2016.08.151.

Zhang, L., Lyu, C., Hinds, G., Wang, L., Luo, W., Zheng, J., Ma, K., 2014. Parameter Sensitivity Analysis of Cylindrical LiFePO 4 Battery Performance Using Multi-Physics Modeling . Journal of The Electrochemical Society 161, A762–A776. doi:10.1149/2.048405jes.

Zhao, R., Gu, J., Liu, J., 2014. An investigation on the significance of reversible heat to the thermal behavior of lithium ion battery through simulations. Journal of Power Sources 266, 422–432. doi:10.1016/j.jpowsour.2014.05.034.